ELSEVIER

J. Non-Newtonian Fluid Mech. 142 (2007) 143–149

Journal of Non-Newtonian Fluid Mechanics

www.elsevier.com/locate/jnnfm

Surface tension driven fingering of a viscoplastic film

Neil Balmforth [a], Shilpa Ghadge [b,*], Tim Myers [c]

[a] *Department of Mathematics of Earth & Ocean Sciences, University of British Columbia, Vancouver, BC, Canada*
[b] *Department of Mathematics, University of British Columbia, Vancouver, BC, Canada*
[c] *Department of Mathematics and Applied Mathematics, University of Cape Town, Rondebosch, South Africa*

Received 13 March 2006; received in revised form 24 July 2006; accepted 26 July 2006

Abstract

We investigate surface-tension-driven fingering of a thin layer of viscoplastic fluid. Using standard lubrication theory we derive an equation for the flow of the film which includes effects of surface tension and yield stress. We obtain traveling-wave solutions to model the advance of a steadily propagating front and then apply a linear stability analysis to model finger growth and to determine the effect of the yield stress. Qualitative agreement is demonstrated between the numerical results and experiments.

Keywords: Fingering instability; Viscoplastic fluid; Herschel–Bulkley relation; Contact line; Thin films; Linear stability analysis

1. Introduction

The moving contact line of a thin fluid film usually breaks into fingers. This behaviour can be troublesome in industrial applications as it may lead to the formation of dry spots or affect the quality of surface coatings. Hence, understanding and controlling the behaviour is of great importance. The fingering of a Newtonian fluid has been studied in detail, both experimentally and theoretically, by numerous researchers (e.g. [1]). The most commonly accepted explanation of the origin of these fingers is in terms of the instability of a steadily moving front: For a gravity-driven film advancing over a dry surface, surface tension holds up fluid in the vicinity of the contact line, leading to a distinctive capillary "ridge". If this ridge is sufficiently thick, then the front becomes gravitationally unstable to perturbations with structure parallel to the contact line, causing the advancing front to break up into fingers [2–4]. A useful summary of fingering in gravity-driven Newtonian films is provided by Kondic [5].

The majority of previous work on fingering deals with Newtonian fluids. However, many fluids of industrial and geophysical importance are non-Newtonian. In this paper we focus on fingering in viscoplastic fluid films. For viscoplastic fluids, it has been observed that the yield strength in the fluid reduces the number of fingers on the contact line, and that the contact line becomes stable at a critical yield stress [6]. This trend is corroborated by a suite of our own experiments which are illustrated in Fig. 1. The topmost picture shows a film of silicon oil, which is a Newtonian fluid, propagating down a slope. The following pictures show flow under identical conditions but with increasing amounts of kaolin added to the oil. As the kaolin concentration increases there is an obvious reduction in the number and amplitude of the fingers. Kaolin plausibly adds a yield strength to the fluid whilst leaving its surface tension roughly the same (although the detailed properties of kaolin suspended in oil are not known). However, the main conclusion we wish to draw from these experiments is that they suggest the fingering instability could be avoided by making a fluid viscoplastic. This would clearly be advantageous in many industrial applications.

In the rest of this paper we adopt a more theoretical approach to the problem and examine the stability of the moving front via a linear stability analysis. We take advantage of the lubrication approximation to simplify the governing fluid equations. The resulting equation for the depth of the thin film offers a compact setting to construct steadily propagating planar fronts and test their linear stability. We conclude with a brief comparison with experiments.

2. Mathematical model

Consider a thin film of incompressible fluid flowing down a plane inclined at an angle ϕ to the horizontal. We choose the

* Corresponding author. Tel.: +1 604 827 3296.
E-mail address: shilpa@math.ubc.ca (S. Ghadge).

0377-0257/$ – see front matter © 2006 Elsevier B.V. All rights reserved.
doi:10.1016/j.jnnfm.2006.07.011

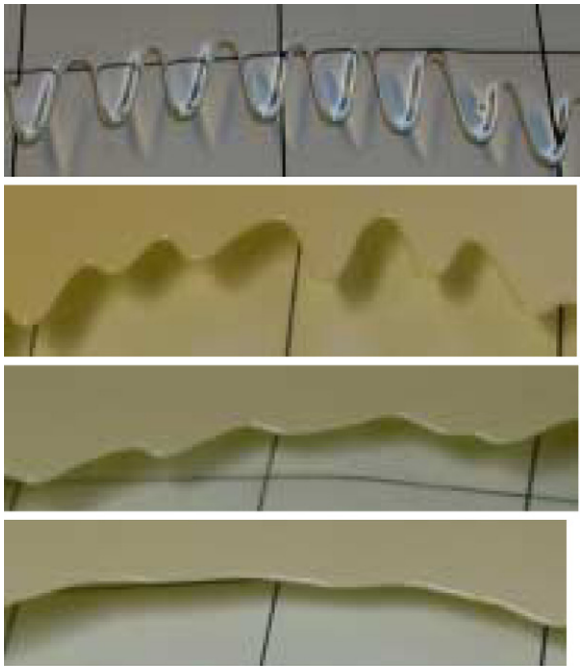

Fig. 1. Fingering patterns obtained on a plane inclined at an angle $\phi = 25^\circ$. The topmost picture is of silicon oil with viscosity 500 cSt. The lower pictures show kaolin suspensions in the oil with concentrations of 15, 17 and 20 wt.%, respectively.

coordinate system such that the fluid sheet flows over the x–y plane with x taken along the down-slope direction, and z normal to the slope, as shown in Fig. 2. The film depth is denoted by $h(x, y, t)$ and the flow is described by the velocity field $\mathbf{u}(\mathbf{x}, t) = (u, v, w)$; ρ denotes the density, $p(\mathbf{x}, t)$ is the pressure field and g is the gravitational acceleration.

The flow is described by the usual equations expressing conservation of mass and momentum, coupled with a suitable constitutive law. We do not use these equations in their full glory, but, following the usual path of lubrication theory (see the articles by Ancey [7] and Balmforth et al. [8]), we immediately skip to a simplified, dimensionless version. In dimensionless form, the abridged conservation of mass and momentum are

$$\nabla \cdot \mathbf{u} = 0, \tag{1}$$

$$-\frac{\partial p}{\partial x} + \frac{\partial}{\partial z}\tau_{xz} + 1 = 0, \tag{2}$$

$$-\frac{\partial p}{\partial y} + \frac{\partial}{\partial z}\tau_{yz} = 0, \tag{3}$$

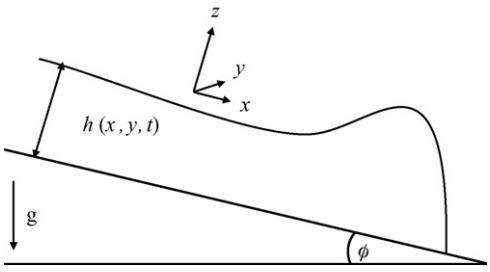

Fig. 2. A schematic illustration of the fluid geometry.

$$-\frac{\partial p}{\partial z} - 1 = 0. \tag{4}$$

Eqs. (2)–(4) indicate that the dominant force balance involves the two shear stresses, τ_{xz} and τ_{yz}, and the fluid pressure. The constant terms represent the effect of gravity in the x and z directions. To non-dimensionalize the equations in this way, we have scaled z with a characteristic depth, H, and used an in-plane length scale, $L = H/\tan\phi$, for x and y. We assume $\phi \ll 1$, so that $H \ll L$ and therefore model flow down a shallow slope, although it is a simple matter to re-scale and deal with a steeper incline. The scales for pressure and shear stresses are chosen to be $\rho g H \cos\phi$ and $\rho g H \sin\phi$, respectively.

We model the rheology of the viscoplastic fluid using the Herschel–Bulkley law [7,8]. This constitutive relation contains a yield stress, τ_p, and a nonlinear viscosity, $K\dot{\gamma}^{n-1}$, where K is the consistency, n a power-law index, and $\dot{\gamma}$ measures the deformation rate (it is the second invariant of the rate of strain tensor). In the thin layer limit, the full three-dimensional form of the law can be reduced to the simpler, dimensionless prescription:

$$(\tau_{xz}, \tau_{yz}) = \left(\dot{\gamma}^{n-1} + \frac{Bn}{\dot{\gamma}}\right)(u_z, v_z), \quad \tau > Bn, \tag{5}$$

$$\dot{\gamma} = 0, \quad \tau < Bn, \tag{6}$$

$$\dot{\gamma} \equiv \sqrt{u_z^2 + v_z^2}, \quad \tau \equiv \sqrt{\tau_{xz}^2 + \tau_{yz}^2}, \tag{7}$$

where $Bn = \tau_p H^n / K U^n$ is the Bingham number, $U = gH^3 \cos\phi/\nu L$ a characteristic speed, and $\nu = K(U/H)^{n-1}/\rho$ is an effective kinematic viscosity.

The no-slip boundary condition, $u = w = 0$, is applied on the plane $z = 0$. At the front of the fluid, one would ideally like to impose $h \to 0$. However, this leads to a singularity in the stresses and a conflict between the no-slip condition and the need for the fluid edge to advance. We avoid this 'contact line paradox' by pre-wetting the inclined plane, $h = \delta$ for $x \to \infty$, where $\delta \ll 1$ is thickness of the precursor film. An unfortunate aspect of the problem is that there are technical mathematical difficulties in the limit $\delta \to 0$ which have the consequence that one simply cannot ignore this parameter even when small (see later discussion and [9]).

The free surface, $z = h(x, y, t)$, is assumed to be stress free. For our thin film, this translates to the two conditions:

$$\tau_{xz} = \tau_{yz} = 0. \tag{8}$$

The pressure jump across the free surface is proportional to the curvature and, in the lubrication limit, gives

$$p = C\nabla^2 h, \tag{9}$$

where $C = \sigma H^3/\rho\nu U L^3$ is the inverse capillary number, σ being the surface tension. We also impose the kinematic condition:

$$w = h_t + uh_x + vh_y. \tag{10}$$

Integrating Eq. (4), subject to (9), determines the pressure:

$$p = h - z - C\nabla^2 h. \tag{11}$$

Eqs. (2) and (3) may also be integrated immediately and in conjunction with the constitutive law, we find

$$\tau_{xz} = \left(\dot\gamma^{n-1} + \frac{Bn}{\dot\gamma}\right) u_z = (1-p_x)(h-z), \tag{12}$$

$$\tau_{yz} = \left(\dot\gamma^{n-1} + \frac{Bn}{\dot\gamma}\right) v_z = -p_y(h-z). \tag{13}$$

Using the definition of τ from (7) together with Eqs. (12) and (13), we obtain the relation:

$$\tau = \Gamma(h-z) = \dot\gamma^n + Bn, \quad \Gamma = \sqrt{(1-p_x)^2 + p_y^2}. \tag{14}$$

These expressions are based on the assumption that the fluid is deforming, i.e. the yield stress is exceeded $\tau = \Gamma(h-z) > Bn$; otherwise we should set $u_z = v_z = 0$. This leads to the definition of a 'yield surface' $z = Y(x, y, t)$ which partitions a plug-like region from a fully yielded flow, defined by

$$Y = \max\left\{h - \frac{Bn}{\Gamma}, 0\right\}. \tag{15}$$

This prediction leads to a paradox since the fluid is spreading on the inclined plane, and the plug region cannot be rigid. Higher orders of the lubrication model resolve this paradox by showing that the stresses above the surface Y are slightly greater than the yield stress Bn, see [10], and hence there is no true plug region. In other words, the region above Y appears to be solid to leading order but is actually weakly yielding; hence it is called a 'pseudo plug' and the dividing surface a 'fake yield surface'.

Note that, if $h < Bn/\Gamma$, the pseudo plug occupies the entire fluid layer. In fact, in this situation the gravitational force acting on the fluid is insufficient to cause it to yield at all, and the pseudo plug is actually a real motionless plug. This is of particular relevance at the precursor film where we have $h = \delta \ll 1$. We therefore expect stagnant regions to exist ahead of the advancing fluid front. We automatically incorporate this true yield condition by requiring $Y = 0$ if $h < Bn/\Gamma$, as indicated in (15).

Integrating the continuity equation in z from $z = 0$ to h and applying the kinematic condition at $z = h$, we obtain the mass balance relation:

$$\frac{\partial h}{\partial t} + \nabla\cdot\mathbf{Q} = 0, \tag{16}$$

where the flux $\mathbf{Q}$ is given by

$$\mathbf{Q} = \int_0^h \begin{pmatrix} u \\ v \end{pmatrix} \mathrm{d}z = \int_0^h (h-z)\begin{pmatrix} u_z \\ v_z \end{pmatrix} \mathrm{d}z$$
$$= \begin{pmatrix} 1-p_x \\ -p_y \end{pmatrix} \int_0^h (h-z)\frac{\dot\gamma}{\Gamma}\mathrm{d}z. \tag{17}$$

Thus, we arrive at our thin-layer equation:

$$\frac{\partial h}{\partial t} + \frac{\partial}{\partial x}\left[\frac{n\Gamma^{(1/n)-1}Y^{1+(1/n)}}{(n+1)(2n+1)}(2nh+h-nY)(1-p_x)\right]$$
$$- \frac{\partial}{\partial y}\left[\frac{n\Gamma^{(1/n)-1}Y^{1+(1/n)}}{(n+1)(2n+1)}(2nh+h-nY)p_y\right] = 0. \tag{18}$$

The thin-layer equation (18) takes the form of a nonlinear diffusion equation. For simplicity, in what follows we consider the case $n = 1$, i.e. the Bingham fluid. In this case, (18) reduces to

$$\frac{\partial h}{\partial t} + \frac{\partial}{\partial x}\left[\frac{Y^2}{6}(3h-Y)(1-p_x)\right] - \frac{\partial}{\partial y}\left[\frac{Y^2}{6}(3h-Y)p_y\right] = 0. \tag{19}$$

It further reduces to the standard Newtonian equation explored in the past if we set $Bn = 0$, which gives $Y = h$ (implying the film has no stagnant regions) and $(3h-Y)Y^2/6 = h^3/3$. For the Newtonian problem, the mathematical troubles associated with the limit, $h \to 0$ (mentioned above and described later in more detail), come about because the diffusivity, $h^3/3$, vanishes if we put $h = \delta = 0$ ahead of the fluid front. Perhaps the most common practice to avoid such troubles is to impose a precursor film and fix $\delta > 0$. For the viscoplastic problem, we follow suit and also consider a finite precursor film. Unfortunately, because our effective diffusivity is now $(3h-Y)Y^2/6$, this trick is not sufficient: the diffusivity may still vanish for $Y = 0$ even if h is kept finite. In other words, the mathematical troubles that plague the Newtonian problem at the contact line, return to haunt us at the yield point, $Y = 0$; the precursor film does not help. We must, therefore, find another way to prevent the diffusivity from vanishing. A convenient cure is to regularize the Bingham model.

2.1. Regularization of the constitutive relation

To avoid the problem with $Y \to 0$ in the thin-layer equation, we turn to a regularized version of the Bingham constitutive relation, which allows a fluid to deform very slightly below the yield stress. Instead of (5) and (6), we now set

$$(\tau_{xz}, \tau_{yz}) = \left(1 + \frac{Bn}{\dot\gamma + \varepsilon}\right)(u_z, v_z), \tag{20}$$

where $\varepsilon \ll 1$ is a regularization parameter. In the limit $\dot\gamma \gg \varepsilon$, this model reduces to the Bingham model and in the limit $\dot\gamma \ll \varepsilon$, it gives a highly viscous Newtonian behaviour as shown in Fig. 3. Other models have been suggested to regularize the Bingham constitutive relation (see [11]); we use (20) because it leads to an analytical thin fluid equation generalizing (19).

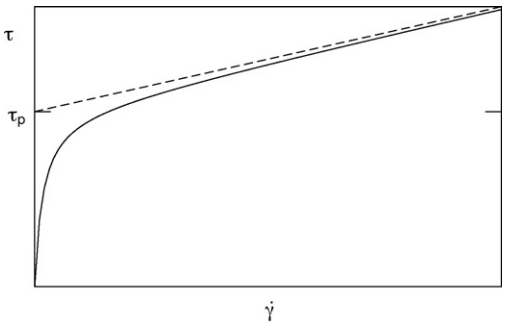

Fig. 3. The regularized constitutive law (20). The dotted line shows the Bingham model.

Using (20), we obtain a quadratic relation between τ and $\dot\gamma$:

$$\tau = \left(1 + \frac{Bn}{\dot\gamma + \varepsilon}\right)\dot\gamma \tag{21}$$

or

$$2\dot\gamma = \tau - Bn - \varepsilon + \sqrt{(\tau - Bn - \varepsilon)^2 + 4\varepsilon\tau}. \tag{22}$$

Solving the equations much as before, we eventually find

$$\frac{\partial h}{\partial t} + \frac{\partial}{\partial x}[(1 - p_x)F] + \frac{\partial}{\partial y}[-p_y F] = 0, \tag{23}$$

where

$$F(h, \Gamma) = \frac{1}{6}\left([(h - Z)^2 + T]^{3/2} - (Z^2 + T)^{3/2}\right) + \frac{h^2}{12}(3\bar Y - h) + \frac{TZ}{8}[S_2 - S_1 + 2(\theta_2 - \theta_1)],$$

$$\bar Y = h - \frac{Bn + \varepsilon}{\Gamma}, \quad Z = \frac{Bn - \varepsilon}{\Gamma}, \quad T = \frac{4\varepsilon\, Bn}{\Gamma^2},$$

$$S_1 = \sinh 2\theta_1, \quad S_2 = \sinh 2\theta_2, \quad \sinh\theta_1 = -\frac{Z}{\sqrt{T}},$$

$$\sinh\theta_2 = \frac{h - Z}{\sqrt{T}}. \tag{24}$$

In the limit, $\bar Y \gg \varepsilon \to 0$, $F \to (3h - Y)Y^2/6$, and we recover the Bingham model (19). Conversely, for $h < Bn/\Gamma$ and $\varepsilon \ll 1$, we recover a viscous problem with $F \to \varepsilon h^3/3Bn$.

3. Planar fronts

We now look for steadily propagating planar front solutions (i.e. constant in the y-direction) to (23). To find them, we transform into a moving coordinate system which is traveling at a constant velocity, V, in the x-direction and introduce a new coordinate, $\xi = x - Vt$. The solution, $h = h_0(\xi)$, is steady in this reference frame and satisfies

$$d + Vh_0 = F(h_0, \Gamma_0)\Gamma_0\,\mathrm{sgn}(1 - h_{0\xi} + Ch_{0\xi\xi\xi}),$$
$$\Gamma_0 = |1 - h_{0\xi} + Ch_{0\xi\xi\xi}|, \tag{25}$$

where d is a constant of integration. We obtain V and d by matching the solution onto a constant film height behind the front and the precursor layer in front, $h_0 \to 1$ as $\xi \to -\infty$ and $h_0 \to \delta$ as $\xi \to \infty$:

$$(1 - \delta)V = F(1, 1) - F(\delta, 1),$$
$$(1 - \delta)d = F(\delta, 1) - \delta F(1, 1). \tag{26}$$

Given V and d and the functional form of F in (24), the first relation in (25) determines Γ_0 algebraically in terms of the depth profile, $h_0(\xi)$. The second relation in (25) then provides an ordinary differential equation for $h_0(\xi)$. In other words, (25) is a coupled, algebraic-differential system to be solved for the steady front profile. For the boundary conditions, we patch the solution onto exponentially decaying tails on either side of the front, and break the translational invariance by imposing $h_0 = 1$ at the left end.

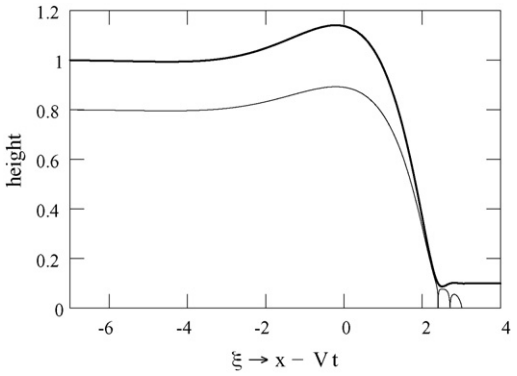

Fig. 4. Fluid depth, h_0 is represented by a thick line, and yield surface, $\bar Y(\xi)$ is represented by a thin solid line, for a front with $\delta = 0.1$, $Bn = 0.1$, $C = 1$ and $\varepsilon = 10^{-3}$.

In Fig. 4 we show a solution of (25), together with the "yield surface", $\bar Y(\xi) = h - (Bn + \varepsilon)/\Gamma$. Note that with the regularized model, the fluid yields everywhere, i.e. there is no fully stagnant region even in the precursor film. Thus, where $\bar Y < 0$, we have a sluggish domain in the fluid rather than a rigid one. All of the precursor film is in such a sluggish domain, in keeping with the idea that gravity is insufficient to cause significant flow there. The oscillations in $\bar Y$ near the front are due to the corresponding variations in h and its derivatives there, which are in turn generated by the surface tension (as in the Newtonian problem). The oscillations in $\bar Y$ are more marked than in h, which gives a curious looking structure to the flow front. However, one should bear in mind that, in the regularized model, $\bar Y$ appears as an auxiliary mathematical variable with no immediate physical significance; by analogy with the Bingham model, we see that $\bar Y$ can be interpreted as a guide for where one expects the fluid to be weakly shearing. Nevertheless, the precise location of $\bar Y$ is not of special significance, and the oscillations at the flow front mainly indicate that the precursor film and the transitional region adjacent to it have little shear.

From Fig. 5, we see that as we increase the Bingham number, the size of the ridge near the contact line becomes smaller. Because the capillary ridge is crucial to fingering instability, this suggests that yield strength is stabilizing. However, we must await proper stability analysis before we can draw this conclusion with certainty.

The mathematical formulation of the problem contains three other parameters besides the Bingham number, C, δ and ε. The capillary number controls the effect of surface tension; to avoid too large a search through parameter space, and because we are interested in fronts for which surface tension is always present, we fix $C = 1$. For Newtonian fluids, the effect of the precursor film thickness has been studied in [9]. They show that, as we take the limit $\delta \to 0$, the maximum height of the profile diverges. We also see this effect in the current model with finite Bn: in Fig. 6 we plot the maximum height of the profile against δ for $Bn = 0.1$. Thus, following [9] we also conclude that the solution does not converge as $\delta \to 0$. The remedy for this problem is to introduce the detailed physics of the contact line; here, we simply admit this drawback of the model and fix the parameter δ to 0.1.

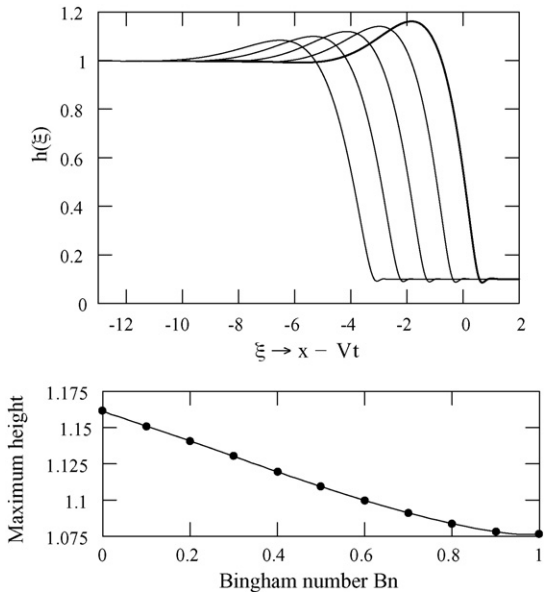

Fig. 5. In the top panel, depth profiles corresponding to different values of the Bingham number are plotted. The Newtonian profile is shown by the bold solid curve. Curves on the left correspond to $Bn = 0.2$, 0.4, 0.6 and 0.8, moving from right to left, respectively. In the bottom panel, the maximum height of h_0 is plotted as a function of the Bingham number Bn.

We plot the maximum profile height against ε for two values of the Bingham number in Fig. 7. As $\varepsilon \to 0$, the maximum height of the profile converges to a certain value (unlike the corresponding limit of δ). From Fig. 7, we draw the important conclusion that the effect of the parameter ε is not significant on the solution provided it is sufficiently small.

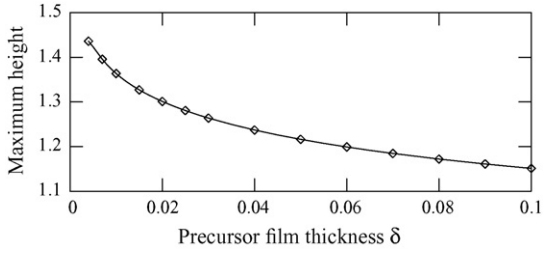

Fig. 6. Maximum height of the front profile against δ. The Bingham number is $Bn = 0.1$, $\varepsilon = 10^{-3}$ and $C = 1$.

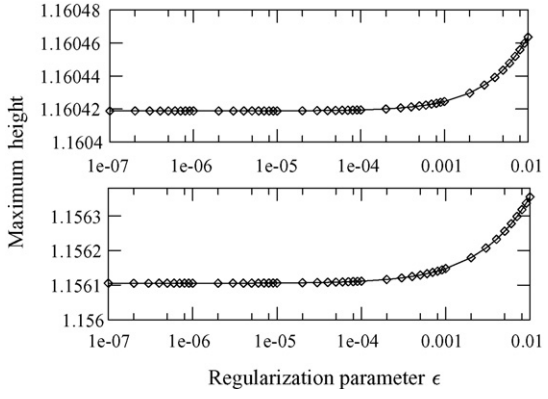

Fig. 7. Maximum height of the front profile against ε. For the upper plot the Bingham number is $Bn = 0.01$, and for lower plot $Bn = 0.05$.

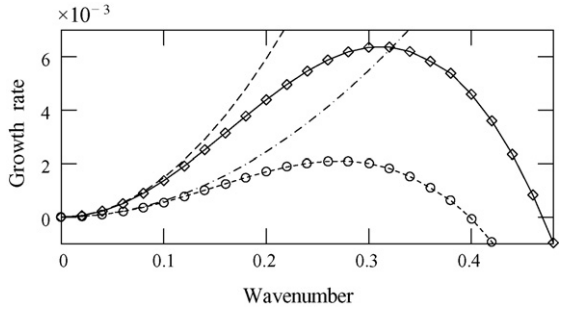

Fig. 8. Growth rate, λ, against wavenumber, l, for two fronts with $Bn = 0.05$ (diamonds) and $Bn = 0.25$ (circles) ($\delta = 0.1$, $C = 1$ and $\epsilon = 10^{-3}$). The dashed curves show the expected growth rates from long-wave theory.

4. Linear stability analysis

To explore the linear stability of the steadily moving front, we set $h = h_0(\xi) + \eta(\xi)\, e^{ily+\lambda t}$, where $\eta \ll h_0$, λ is the growth rate, and the y-dependence of the solution is decomposed into Fourier modes with l as wavenumber. After linearizing about the front, η is found to satisfy the equation:

$$\lambda\eta - V\eta' + Q' + l^2 F[(1 + Cl^2)\eta - C\eta''] = 0, \tag{27}$$

where

$$Q = [F + \Gamma_0 F_\Gamma][C\eta''' - (1 + Cl^2)\eta'] + \frac{Vh_0 + d}{F} F_h \eta.$$

Here primes denotes differentiation with respect to ξ, and F and its derivatives are evaluated at the known front profile $h_0(\xi)$. Again we patch the solution onto exponentially decaying tails to furnish boundary conditions.

Results obtained by numerically solving (27) are presented in Figs. 8 and 9. Fig. 8 shows the growth rate versus wavenumber for particular front solutions with $Bn = 0.05$ and $Bn = 0.25$ ($\delta = 0.1$, $C = 1$ and $\epsilon = 10^{-3}$). The growth rate corresponding to the fastest growing wavenumber decreases as we increase the Bingham number. This is shown in more detail in Fig. 9, where the fastest growing wavenumber and the growth rate corresponding to that wavenumber are plotted against the Bingham number. The maximum growth rate decreases as the Bingham number increases and becomes zero at some critical value of the Bingham number, whereafter all of the modes are stable.

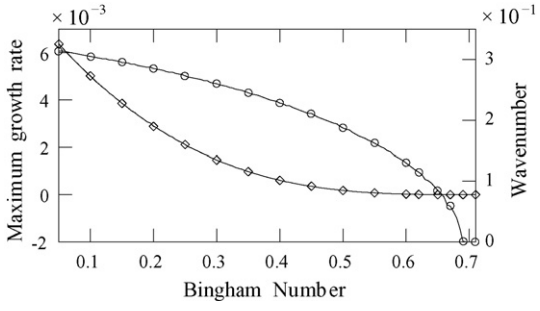

Fig. 9. Wavenumber and growth rate corresponding to the fastest growing mode as a function of Bingham number Bn, with $\varepsilon = 10^{-3}$, $C = 1$ and $\delta = 0.1$. The line with circles corresponds to wavenumber and the line with squares corresponds to growth rate.

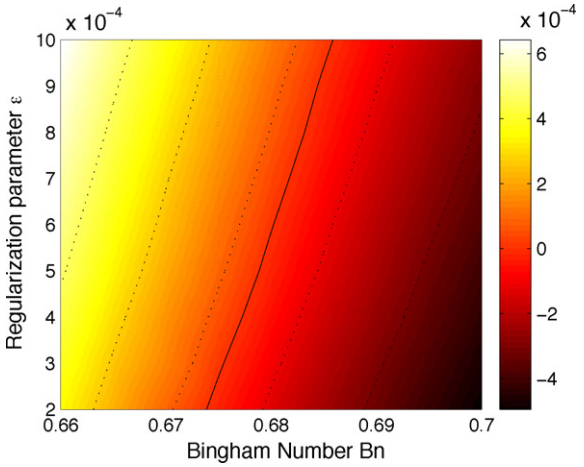

Fig. 10. λ_2 as a density on the (Bn, ε)-plane. The black solid line is the zero contour.

4.1. Long transverse waves

The long-wave (in l) character of the instability found numerically above prompts us to analyze the linear stability problem (27) asymptotically in the limit of small transverse wavenumber. We expand η and λ in even powers of wavenumber l:

$$\eta = \eta_0 + l^2\eta_2 + \cdots, \qquad \lambda = l^2\lambda_2 + \cdots \tag{28}$$

We then substitute (28) in (27). To the leading order, we obtain

$$\mathcal{L}\eta_0 \equiv -V\eta_0' + [(F + F_\Gamma\Gamma_0)(\eta_0' + C\eta_0''') + F_h\eta_0(1 - h_0' + Ch_0''')]' = 0. \tag{29}$$

This equation has the solution $\eta_0 = h_0'$, which corresponds to the translational invariance of the planar front. At the next order, we obtain

$$\mathcal{L}\eta_2 + \lambda_2\eta_0 - C(F + F_\Gamma\Gamma_0)\eta_0 + F(\eta_0 - C\eta_0'') = 0. \tag{30}$$

We impose a solvability condition on this equation by integrating the equation in ξ to obtain

$$\lambda_2 = \frac{1}{1-\delta}\int [F - (Vh - d)]\mathrm{d}x. \tag{31}$$

In Fig. 8, we compare the prediction (31) with the results of numerical computations; the two agree at small l, as expected.

Because the long-wave result (31) involves only the equilibrium front profile, it offers a powerful and convenient tool to detect instability without solving the full linear stability equations with a spectrum of wavenumbers. In particular, we can use (31) to construct the neutral stability boundary. In Fig. 10, we plot the neutral stability curve on the (Bn, ε) plane. Extrapolating that curve, we find a numerical value for the critical Bingham number as $\varepsilon \to 0$: $Bn = 0.67$. In other words, fingering will not occur for $Bn \geq 0.67$ (according to linear theory at least).

5. Discussion

In this paper, we have formulated a thin-layer model of a viscoplastic fluid film. We used this model to construct steadily propagating planar fronts for the case of Bingham fluids and test their linear stability. The linear stability analysis shows that the effect of yield strength in the fluid is stabilizing, confirming the qualitative predictions of de Bruyn et al. [6]. In order to perform the computations leading to this result, we were forced into regularizing the Bingham constitutive relation to avoid mathematical difficulties near the contact line. Those difficulties are familiar from the Newtonian version of the problem, although the viscoplastic theory has its own peculiarities. The regularization adds an extra parameter, ε, to the model. However, we have been able to show that the solutions converge to a limit as $\varepsilon \to 0$, indicating that this parameter is not significant if chosen small enough.

Table 1
Number of fingers, experimentally obtained for different consistencies and inclination angles

Consistency (%)	15°	20°	25°	30°	35°	40°
0	5	9	14	15	19	
15	3	5	10	13	13	
17	0	7	8	11	15	
20	0	0	3	7	9	12

We have also conducted some preliminary experiments with a kaolin suspension in 500 cSt silicon oil released over an inclined plane; examples are shown on Fig. 1. The experiments were performed by varying the angle of inclination of the plane and the concentration of the kaolin in the silicon oil. The number of fingers observed are tabulated in Table 1 as a function of angle and concentration. This data clearly shows that for a constant angle of inclination there is a reduction in the number of fingers as the kaolin concentration increases. In other words, the wavenumber decreases as the concentration increases, which agrees qualitatively with our analytical results if that concentration corresponds to yield stress.

Most fluids with yield stress also show shear thinning effects. An important generalization of the current theory for the future is therefore to move to the Herschel–Bulkley constitutive model. It is also necessary to advance beyond linear stability theory and explore the ramifications of yield stress on the nonlinear fingering dynamics. For example, although we see a certain characteristic finger wavelength emerging first on the inclined plane, as the film evolves further, the fingers merge and adjust that wavelength to create finite-amplitude patterns which linear theory is inadequate to predict. Finally, it would be worthwhile to perform more quantitative experiments to compare with theory. A key problem, however, is how to set δ and parameterize the physics of the contact line.

References

[1] H. Huppert, Flow and instability of a viscous current down a slope, Nature 300 (1982) 427–429.
[2] S. Troian, E. Herbolzheimer, S. Safran, J. Joanny, Fingering instabilities of driven spreading films, Europhys. Lett. 10 (1989) 25–30.
[3] L. Hocking, M. Miksis, Stability of a ridge of fluid, J. Fluid Mech. 247 (1993) 157–177.
[4] M. Spaid, G. Homsy, Stability of Newtonian and viscoelastic dynamic contact lines, Phys. Fluids 8 (1996) 460–478.

[5] L. Kondic, Instabilities in gravity driven flow of thin fluid films, Siam Rev. 45 (1) (2003) 95–115.
[6] J. de Bruyn, P. Habdas, S. Kim, Fingering instability of a sheet of yield-stress fluid, Phys. Rev. E 66 (2002) 031504.
[7] C. Ancey, Plasticity and geophysical flows. J. Non-Newtonian Fluid Mech. 142 (2007) 4–35.
[8] N.J. Balmforth, R.V. Craster, A.C. Rust, R. Sassi, Viscoplastic flow over an inclined surface. J. Non-Newtonian Fluid Mech. 142 (2007) 219–243.
[9] E. Tuck, L. Schwartz, A numerical and asymptotic study of some third-order ordinary differential equations relevant to draining and coating flows, SIAM Rev. 32 (1990) 453–469.
[10] N.J. Balmforth, R.V. Craster, A consistent thin-layer theory for Bingham plastics, J. Non-Newtonian Fluid Mech. 84 (1999) 65–81.
[11] I.A. Frigaard, C. Nouar, On the usage of viscosity regularisation methods for visco-plastic fluid flow computation, J. Non-Newtonian Fluid Mech. 127 (1) (2005) 1–26.